Submitted to

32nd International Conference on High Energy Physics, ICHEP04, August 16, 2004, Beijing
Abstract: **5-0162**
Parallel Session **5**

www-h1.desy.de/h1/www/publications/conf/conf_list.html

Photoproduction of D^* Mesons at HERA

H1 Collaboration

Abstract

A measurement of cross sections for $D^{*\pm}$ meson photoproduction at HERA is presented. The measurement uses data taken with the H1 detector during the years 1999 to 2000. The cross sections are determined in the kinematic region $171 < W < 256$ GeV, $Q^2 < 0.01$ GeV^2, $p_t(D^*) > 2.5$ GeV, and $|\eta(D^*)| < 1.5$, where W is the photon-proton centre of mass energy and Q^2 is the photon virtuality. Photoproduction is assured through the detection of the scattered electron at small angles. In addition to the total cross section, the data are presented as a function of $p_t(D^*)$, $\eta(D^*)$ and W. The results are compared to QCD predictions in leading order and next-to-leading order using collinear factorisation and to QCD predictions using k_t-factorisation.

1 Introduction

In electron proton interactions heavy quarks are produced predominantly in photon gluon fusion processes, where a photon emitted by the incoming electron interacts with a gluon in the proton forming a quark antiquark pair. The cross section is dominated by processes where the virtuality Q^2 of the exchanged photon is very small. As the heavy quark mass provides a hard scale, heavy quark photoproduction is a good testing ground for QCD calculations.

Charm quark photoproduction has previously been studied at HERA using D^* mesons [1–3]. The measurement of the H1 collaboration [1] was compared to next-to-leading order (NLO) calculations in the "massive" scheme [4,5] using the MRST1 [6] parton density parametrisation of the proton. Within large statistical errors agreement was found.

In this paper differential cross sections for D^* photoproduction obtained from a larger data set are presented in the range $171 < W < 256$ GeV of the photon proton centre of mass energy. The results are compared with the same "massive" NLO calculations using the CTEQ5D [7] proton parton density parametrisation, with NLO calculations in the massless [8] and the fixed-order next-to-leading-logarithmic (FONLL) scheme [9], with a leading order Monte Carlo model incorporating parton showers (PYTHIA [10]) and with predictions from k_t-factorisation and CCFM [11–14] parton evolution as implemented in CASCADE [15, 16].

2 Data Selection

The analysis was performed with data taken in the 1999 and 2000 running periods, when HERA collided positrons[1] with energy $E_e = 27.5$ GeV and protons with $E_p = 920$ GeV. The data set used in this analysis corresponds to an integrated luminosity of 49.2 pb^{-1}.

Photoproduction events are selected by detection of the scattered electron in an electron tagger close to the beam line 33 m away from the interaction point. The small scattering angle leads to a photon virtuality $Q^2 < 0.01$ GeV^2. The acceptance of the tagger depends on the beam position and the inelasticity y, which is reconstructed here using $y = 1 - E_{e'}/E_e$, where $E_{e'}$ is the reconstructed energy of the scattered electron. Restricting the kinematical region to $0.29 < y < 0.65$ (i.e. $171 < W < 256$ GeV) leads to a minimal acceptance of 10%.

The D^* meson is reconstructed via the decay channel[2] $D^{*+} \to D^0\pi_s^+ \to K^-\pi^+\pi_s^+$. Due to the small difference between the D^* and the D^0 masses, $\Delta m = m_{K\pi\pi_s} - m_{K\pi} = 145.4$ MeV, the momentum of the pion produced in the decay of the D^* is very small, strongly restricting the possible kinematic range of the two decay particles. Therefore the combinatorial background is small and a clear signal is obtained.

In each event, tracks with opposite charges were combined in pairs, one assigned the pion, one the kaon mass. If the kaon (pion) assigned track fulfills $p_t(K) > 0.5$ GeV ($p_t(\pi) > 0.3$ GeV), the invariant mass, $m(K\pi)$, is calculated. If the result is consistent with the D^0 mass, $|m(K\pi) - m(D^0)| < 80$ MeV, the remaining tracks with $p_t(\pi_s) > 0.12$ GeV and an opposite

[1] Positrons are generally referred to as electrons in the following.
[2] Charge conjugate states are always implicitly included.

charge to that taken as a kaon are added to form a D^* candidate. It is required to satisfy $p_t(D^*) > 2.5$ GeV and $|\eta(D^*)| < 1.5$. Figure 1 shows the Δm distribution for the remaining D^* candidates. The number of D^* mesons is determined by a fit of a gaussian signal and a three parameter background function. The fit results in 1117$\pm$76 D^* mesons.

3 Cross Sections

Cross sections are presented for inclusive D^* production via the process $ep \to e' D^{*\pm} X$. The kinematic region is $Q^2 < 0.01$ GeV^2, $171 < W < 256$ GeV, $p_t(D^*) > 2.5$ GeV and $|\eta(D^*)| < 1.5$. The cross section differential in a variable Y is calculated from

$$\frac{d\sigma}{dY} = \frac{1}{\mathcal{L} \cdot \mathcal{B} \cdot \epsilon_r \cdot \epsilon_t \cdot \mathcal{A}} \cdot \frac{\Delta N}{\Delta Y}$$

and similarly for the total cross section. ΔN is the number of D^* mesons[3] in a bin of width ΔY, ϵ_r is the reconstruction efficiency (also accounting for kinematic migrations), ϵ_t is the trigger efficiency and $\mathcal{A}$ the mean acceptance of the tagger. $\mathcal{L}$ and $\mathcal{B}$ are the integrated luminosity and the product of the $D^{*+} \to D^0 \pi_s^+$ and $D^0 \to K^- \pi^+$ branching ratios (2.57$\pm$ 0.06% [17]), respectively. To determine ϵ_r a sample of Monte Carlo events generated with PYTHIA [10] are processed by the standard H1 simulation and reconstruction program.

The total inclusive D^* production cross section in the kinematic range specified above amounts to

$$\sigma(D^*) = (4.74 \pm 0.32 \pm 0.64)\ \text{nb}.$$

The first error represents the statistical, the second the systematic uncertainty. The differential cross sections $d\sigma/dp_t$, $d\sigma/d\eta$ and $d\sigma/dW$ are shown in figures 2, 3 and 4.

For the determination of the systematic uncertainty several sources are taken into account and added in quadrature. The uncertainty of the fit yielding the number of D^*-mesons is estimated by subtracting the Δm distribution of wrong charge combinations from the real Δm distribution in the signal region. The model dependence of the reconstruction efficiency is estimated by using a second Monte Carlo sample generated by CASCADE [15, 16]. The most prominent source is the uncertainty on the track reconstruction efficiency (11%). The lowest W-bin has a comparable contribution from the uncertainty of the absolute energy scale in the electron tagger, which is relevant for the acceptance determination. Contributions from the luminosity measurement, the trigger efficiency and the branching ratio amount to 4.4%. These normalisation uncertainties are not taken included in the plotted differential cross sections.

4 Comparison with QCD Calculations

The measured cross sections are compared with next-to-leading order (NLO) calculations in the "3-flavour massive", the "4-flavour massless" and the "matched" (FONLL) scheme and with

[3] Events containing both a D^{*+}- and a D^{*-}-meson are counted twice.

leading order Monte Carlo models. All NLO calculations and the PYTHIA leading order model apply collinear factorisation while the CASCADE leading order model applies k_t-factorisation. The charm mass is always set to $m_c = 1.5$ GeV.

For the "3-flavour massive" scheme [4, 5] the Peterson parametrisation [18] has been used to model the charm fragmentation with $\epsilon_{pet} = 0.035$. The renormalisation and the factorisation scales have been chosen as $2{\cdot}\mu_r = \mu_f = 2{\cdot}\sqrt{m_c^2 + p_{t,c}^2}$. As parton densities CTEQ5D [7] for the proton and GRV-G HO [19] for the photon have been used. The fraction of c-quarks hadronising as D^{*+}-mesons has been set to $f(c \to D^{*+}) = 0.235$ [20]. To estimate the uncertainty of the calculation, the renormalisation scale has been varied by a factor 0.5 (2.0) as an upper (lower) limit. The total cross section in the visible range is $\sigma(D^*)$ = $\left(3.06^{+1.01}_{-0.57}\right)$ nb, which lies slightly below the measured value, but is compatible with the data within errors for the extreme value of μ_r.

The BKK O [21] fragmentation function has been applied for the "4-flavour massless" scheme [8] and the renormalisation and factorisation scales have been chosen as $\mu_r = \mu_f = 2 \cdot \sqrt{m_c^2 + p_{t,c}^2}$ for the central prediction. As parton densities CTEQ6M [22] for the proton and AFG [23] for the photon have been used. To estimate the uncertainty of the calculation, the renormalisation and the factorisation scale have been varied independently as well as simultaneously by a factor 0.5 or 2. The largest deviations from the central value are taken for the quoted uncertainties.

The FONLL [9] calculation has been carried out at $\mu_r = \mu_f = \sqrt{m_c^2 + p_{t,c}^2}$. The fragmentation is done following a fit [24] to the Kartvelishvili [25] ansatz. The parton density parametrisations CTEQ5M [7] for the proton and GRV [19] for the photon have been used and $f(c \to D^{*+}) = 0.235$ [20] applied. The uncertainty is estimated by varying μ_r by factors 0.5 and 2.

Figure 2a) and b) compare the $d\sigma/dp_t$-calculations of all three NLO schemes to the data. The "3-flavour massive" prediction lies below the data in the low p_t regime, where FONLL is closer to the data and "4-flavour massless" fits best. The $d\sigma/d\eta$-calculations for "3-flavour massive" and "4-flavour massless" are shown in figure 3a). Neither calculation can describe the shape of the measured cross section, which shows an enhancement compared with the theory in the forward direction. Both NLO predictions for $d\sigma/dW$ in figure 4a) can describe the shape of the data.

PYTHIA [10] implements DGLAP evolution and contains contributions from both resolved and direct photon interactions. The resolved component is dominated by the charm excitation process. It is calculated from a matrix element with a massless charm quark originating in the photon. The CTEQ5L [7] and GRV-G LO [19] parametrisations are used for the proton and photon parton densities, respectively. CASCADE [15, 16] applies k_t-factorisation with off-mass-shell matrix elements supplemented with CCFM parton evolution. Resolved photon contributions are not explicitly included, but are effectively simulated due to the lack of k_t-ordering [26]. Both models have in common the Peterson parameter $\epsilon = 0.078$.

The total cross section in the visible range, $\sigma(D^*)$, amounts to 5.9 nb for PYTHIA and 6.2 nb for CASCADE. Both lie slightly above the data. PYTHIA reasonably describes the shape of $d\sigma/dp_t$ while CASCADE is too hard (figure 2b). Neither calculation can reproduce

the shape of $d\sigma/d\eta$ (figure 3b). The PYTHIA prediction is split up into its different production mechanisms: direct, resolved with a light parton from the photon and charm excitation. The charm excitation process is dominant in the problematic forward region. However, changing normalisation of this sub-process does not lead to a better overall description. Both PYTHIA and CASCADE describe the shape of $d\sigma/dW$ quite well within the uncertainties (figure 4b).

5 Summary

Cross sections for inclusive $D^{*\pm}$ photoproduction have been presented in the kinematic region $Q^2 < 0.01$ GeV^2, $171 < W < 256$ GeV, $p_t(D^*) > 2.5$ GeV and $|\eta(D^*)| < 1.5$ as a function of $p_t(D^*)$, $\eta(D^*)$ and W. They have been compared to NLO QCD calculations in the "3-flavour massive", in the "4-flavour massless" and – in the case of $d\sigma/dp_t$ – in the "matched" FONLL scheme as well as to two Monte Carlo models, PYTHIA and CASCADE.

The total cross section calculation lies below the data in the "3-flavour massive" NLO calculation and slightly above the data for both PYTHIA and CASCADE. CASCADE yields a p_t spectrum which is harder than measured. The same is true for the "3-flavour massive" NLO calculation which underestimates the low p_t region, while FONLL and "4-flavour massless" are closer to the data. None of the calculations is able to predict adequately the shape of the $d\sigma/d\eta$, but the shape of $d\sigma/dW$ is described by all.

Acknowledgments

We would like to thank S. Frixione for providing us with the "3-flavour massive" code and the FONLL calculation and B. A. Kniehl for providing us with the "4-flavour massless" calculations.

References

[1] C. Adloff, *et al.* (H1-Collaboration), Nucl. Phys., **B545**, (1999) 21. hep-ex/9812023.

[2] J. Abbiendi, *et al.* (ZEUS-Collaboration), Eur. Phys. J., **C6**, (1999) 67. hep-ex/9807008.

[3] ZEUS-Collaboration, *Measurement of D^* Photoproduction at HERA* in *ICHEP 02* (2002).

[4] S. Frixione, M. L. Mangano, P. Nason, G. Ridolfi, Phys. Lett., **B348**, (1995) 633. hep-ph/9412348.

[5] S. Frixione, P. Nason, G. Ridolfi, Nucl. Phys., **B454**, (1995) 3. hep-ph/9506226.

[6] A. D. Martin, R. G. Roberts, W. J. Stirling, R. S. Thorne, Eur. Phys. J., **C4**, (1998) 463. hep-ph/9803445.

[7] H. L. Lai, *et al.* (CTEQ), Eur. Phys. J., **C12**, (2000) 375. hep-ph/9903282.

[8] B. A. Kniehl, in *14th Topical Conference on Hadron Collider Physics* (eds. M. Erdmann, T. Müller), p. 161 (Springer, Heidelberg, 2003). hep-ph/0211008.

[9] M. Cacciari, S. Frixione, P. Nason, JHEP, **03**, (2001) 006. hep-ph/0102134.

[10] T. Sjöstrand, *et al.*, Comput. Phys. Commun., **135**, (2001) 238. hep-ph/0010017.

[11] M. Ciafaloni, Nucl. Phys., **B296**, (1988) 49.

[12] S. Catani, F. Fiorani, G. Marchesini, Phys. Lett., **B234**, (1990) 339.

[13] S. Catani, F. Fiorani, G. Marchesini, Nucl. Phys., **B336**, (1990) 18.

[14] G. Marchesini, Nucl. Phys., **B445**, (1995) 49. hep-ph/9412327.

[15] H. Jung, G. P. Salam, Eur. Phys. J., **C19**, (2001) 351. hep-ph/0012143.

[16] H. Jung, Comput. Phys. Commun., **143**, (2002) 100. hep-ph/0109102.

[17] K. Hagiwara, *et al.* (Particle Data Group), Phys. Rev., **D66**, (2002) 010001.

[18] C. Peterson, D. Schlatter, I. Schmitt, P. Zerwas, Phys. Rev., **D27**, (1983) 105.

[19] M. Glück, E. Reya, A. Vogt, Phys. Rev., **D46**, (1992) 1973.

[20] L. Gladilin, *Charm Hadron Production Fractions*. hep-ex/9912064.

[21] J. Binnewies, B. A. Kniehl, G. Kramer, Phys. Rev., **D58**, (1998) 014014. hep-ph/9712482.

[22] J. Pumplin, *et al.*, JHEP, **07**, (2002) 012. hep-ph/0201195.

[23] P. Aurenche, J. P. Guillet, M. Fontannaz, Z. Phys., **C64**, (1994) 621. hep-ph/9406382.

[24] M. Cacciari, P. Nason. Unpublished.

[25] V. Kartvelishvili, A. Likoded, V. Petrov, Phys. Lett., **B78**, (1978) 615.

[26] S. P. Baranov, *et al.*, Eur. Phys. J., **C24**, (2002) 425. hep-ph/0203025.

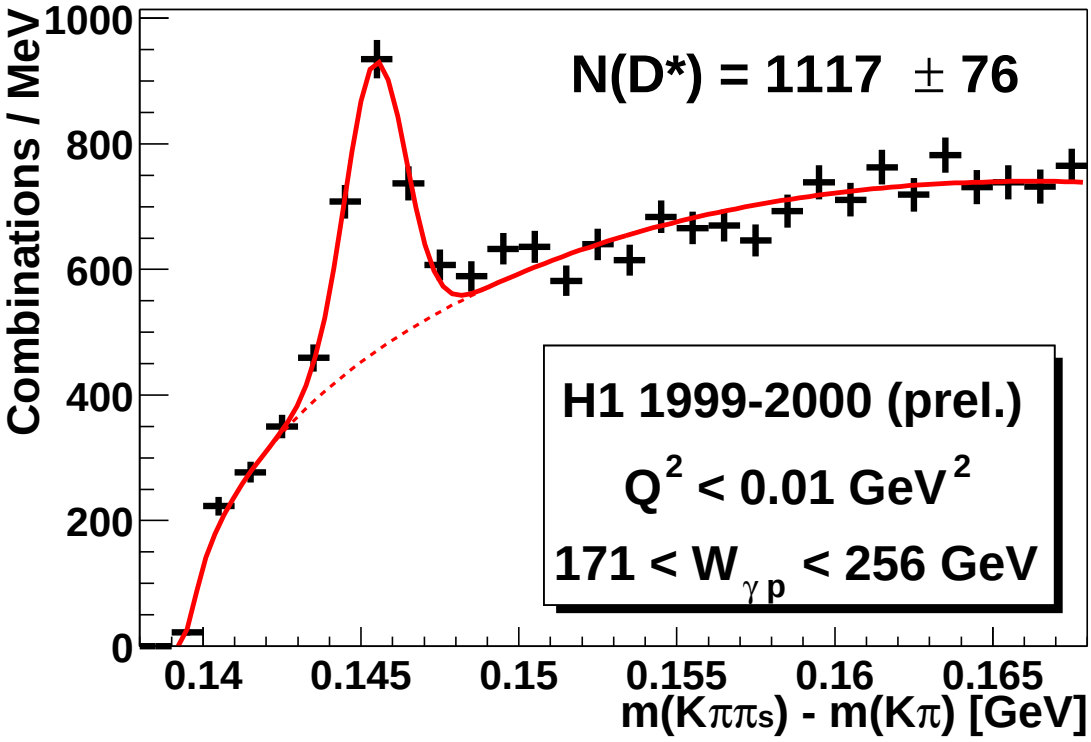

Figure 1: Mass difference $\Delta m = m_{K\pi\pi_s} - m_{K\pi}$ distribution of the D^*-candidates. The solid line represents the result of a fit as described in the text.

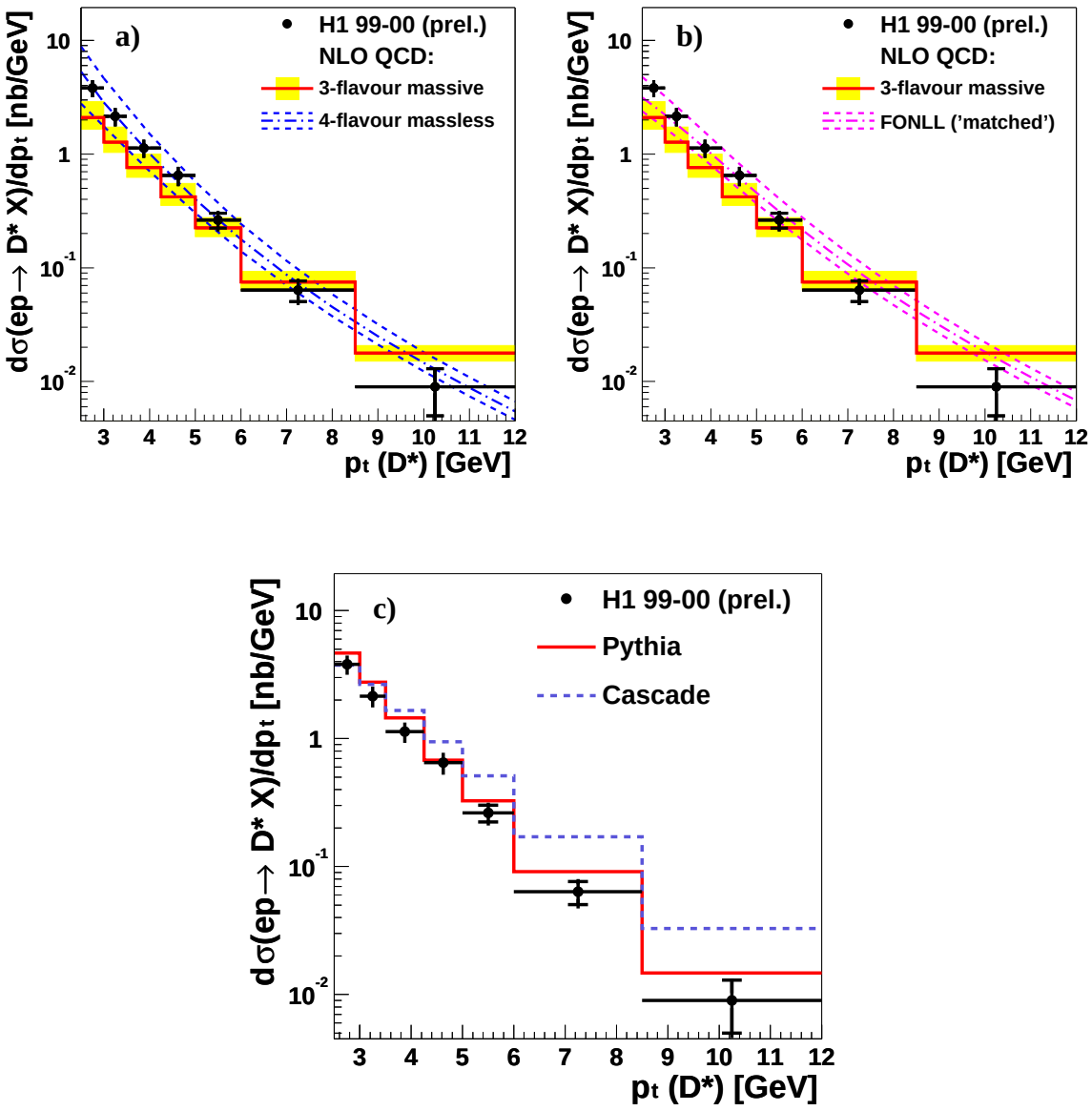

Figure 2: Differential D^*-photoproduction cross section $d\sigma/dp_t$ in the kinematic range $Q^2 <$ 0.01 GeV^2, 171 $< W <$ 256 GeV and $|\eta(D^*)| <$ 1.5. The H1 data are shown as points with error bars (inner: statistical, outer: statistical and systematic added in quadrature). A common normalisation uncertainty of 4.4% is not included. The data are compared with (a) NLO QCD calculations in the "3-flavour massive" and in the "4-flavour massless" scheme, (b) NLO QCD calculations in the "3-flavour massive" and the "matched" FONLL scheme and (c) PYTHIA and CASCADE. The result of the central choice of the parameters of the "3-flavour massive" calculation is shown as a histogram in (a) and (b). The shaded band indicates its uncertainty obtained as described in the text. The "4-flavour massless" and "matched" FONLL calculations are shown as dashed-dotted lines whereas the dashed lines represent their upper (lower) limit.

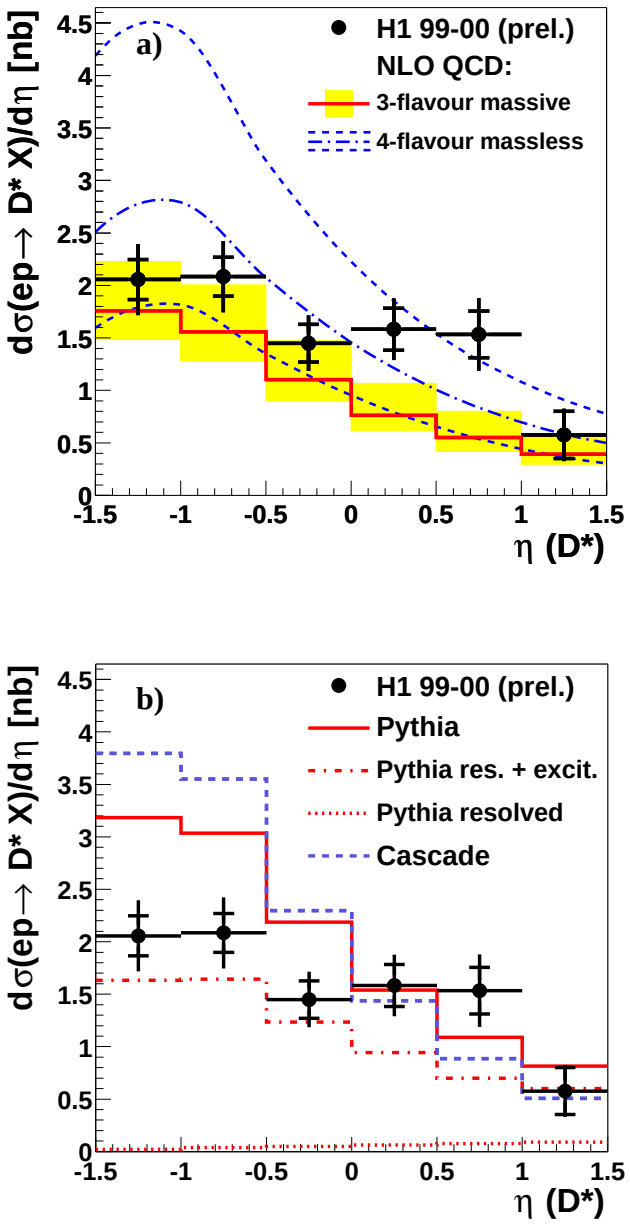

Figure 3: Differential D^*-photoproduction cross section $d\sigma/d\eta$ in the kinematic range $Q^2 < 0.01$ GeV^2, $171 < W < 256$ GeV and $p_t(D^*) > 2.5$ GeV. The H1 data are shown as points with error bars (inner: statistical, outer: statistical and systematic added in quadrature). A common normalisation uncertainty of 4.4% is not included. The data are compared with (a) NLO QCD calculations in the "3-flavour massive" and in the "4-flavour massless" scheme and (b) PYTHIA and CASCADE. The result of the central choice of the parameters of the "3-flavour massive" calculation is shown as a histogram. The shaded band indicates its uncertainty obtained as described in the text. The "4-flavour massless" calculation is shown as the dashed-dotted line whereas the dashed lines represent its upper (lower) limit. PYTHIA is divided into its different components. The dotted line is the resolved photon component from light partons in the photon, the dashed-dotted line adds the charm excitation process and the full line finally adds the direct component.

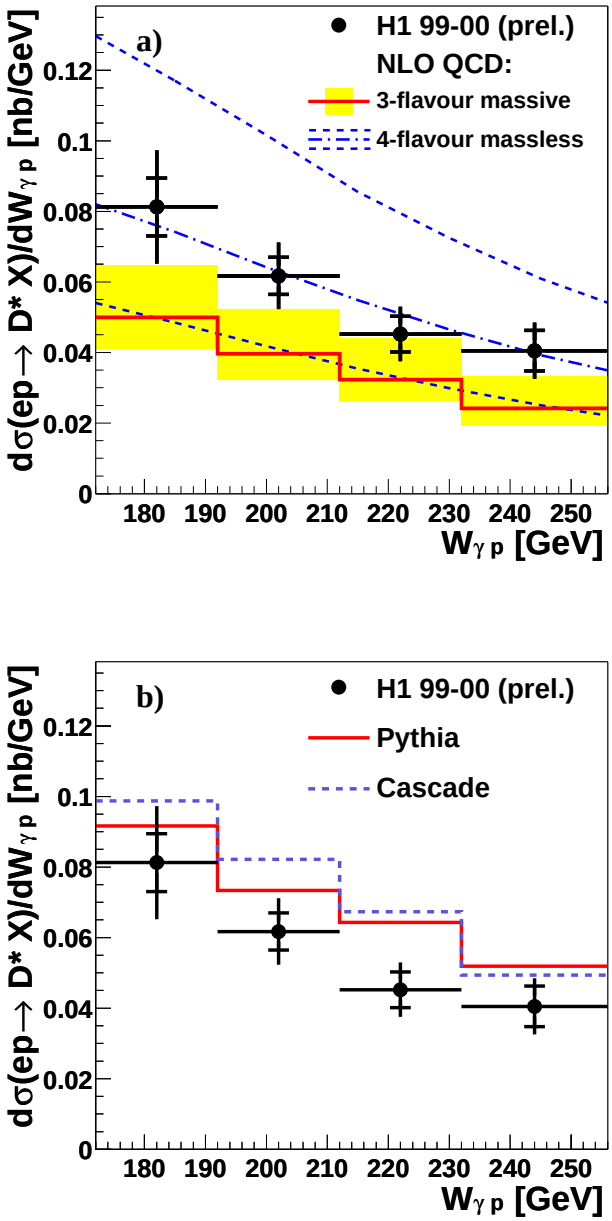

Figure 4: Differential D^*-photoproduction cross section $d\sigma/dW$ in the kinematic range $Q^2 <$ 0.01 GeV^2, $p_t(D^*) > 2.5$ GeV and $|\eta(D^*)| < 1.5$. The H1 data are shown as points with error bars (inner: statistical, outer: statistical and systematic added in quadrature). A common normalisation uncertainty of 4.4% is not included. The data are compared with (a) NLO QCD calculations in the "3-flavour massive" and in the "4-flavour massless" scheme and (b) PYTHIA and CASCADE. The result of the central choice of the parameters of the "3-flavour massive" calculation is shown as a histogram. The shaded band indicates its uncertainty obtained as described in the text. The "4-flavour massless" calculation is shown as dashed-dotted line whereas the dashed lines represent its upper (lower) limit.